Chemistry–A European Journal
Research Article
doi.org/10.1002/chem.202403253
Chemistry Europe
European Chemical Societies Publishing
www.chemeurj.org

Bismuth Bound to Transition Metals: Visible-Light-Induced Olefin Coordination, Reductive Elimination, and Oxidative Addition

Jacqueline Ramler[+],[a] Felix Geist[+],[a] Cornelius Mihm,[b] Lukas Lubczyk,[b] Sascha Reith,[a] Christoph Herok,[c] Felipe Fantuzzi,*[d] and Crispin Lichtenberg*[a]

A series of dibenzobismepinyl ($C_{14}H_{10}Bi$) substituted transition metal complexes of the type [$(C_{14}H_{10}Bi)M(CO)_x(L)$] (M = Mn, Co, Fe) was prepared in salt elimination reactions from a halobismepine and sodium metallates. Irradiation of these complexes with visible light has been investigated, aiming at the elimination of one carbonyl ligand and the concomitant coordination of the bismepine's olefin moiety to the transition metal center. The resulting complexes of the type [$\{\kappa^2C,\kappa^1Bi\text{-}(C_{14}H_{10})Bi\}M(CO)_{x-1}(L)$] (M = Co, Fe) have been isolated and fully characterized. When two dibenzobismepinyl units are positioned in the coordination sphere of an iron carbonyl complex fragment, reductive elimination/oxidative addition events of the dibismuthane $(C_{14}H_{10}Bi)_2$ have been shown to be relevant. The analytical techniques applied in this work include (heteronuclear) NMR spectroscopy, elemental analysis, single-crystal X-ray diffraction analysis, UV/Vis spectroscopy, IR spectroscopy and (TD)-DFT calculations.

Introduction

The utilization of bismuth compounds as ligands in the coordination sphere of main group and transition metals has a longstanding tradition in coordination chemistry.[1–7] Modern approaches have strongly diversified the ligand design in this field of research. Recent developments include bismuth-based Z-type ligands, in which the central atom donates electron density to a vacant bismuth-centered molecular orbital of the ligand, as well as visible-light-driven reactions.[8,9] In another recent approach, the remote control of ligand properties by bismuth atoms has been exploited: the incorporation of bismuth atoms into organic frameworks has been utilized to decisively impact the nature of the resulting ligands by dictating their geometric and electronic properties without Bi—M interactions being realized.[10–13]

In the reactivity and catalytic activity of compounds featuring bismuth-based ligands, it has mostly been the labile nature of Bi–M and Bi–C bonds that gave access to unexpected transformations and significant catalytic activities. This includes the utilization of bismuth compounds as synthons for radical species,[14] low-energy-pathways for heterolytic Bi–C bond cleavage,[13,15] and facile dissociation of bismuthanes from transition metal centers.[16]

The vast majority of bismuth compounds in the coordination sphere of transition metals represents monodentate ligands.[1–7] This is likely due to initial limitations in the synthesis of more complex bismuth compounds with additional functional groups in positions that generate a suitable binding pocket for a transition metal complex fragment. In the conceptualization of bidentate organobismuth ligands, linking a bismuth-based donor site to an olefin functional group as a second coordination point represents an intriguing combination. This would generate a bidentate ligand with two coordination sites that can be classified to show a pronouncedly soft character according to the HSAB principle.[17,18] In addition, olefin ligands have the potential to effectively modulate the electronic properties of central atoms, to grant access to complexes featuring central atoms in unusual oxidation states, and to act as steering ligands in (asymmetric) catalysis.[19]

When aiming at the synthesis of transition metal complexes featuring a hybrid bismuth/olefin ligand, dibenzobismepines appear to be attractive choices.[10,11,17,23–25] Just like their lighter nitrogen and phosphorus homologs, they form a concave structure, thereby exposing the pnictogen atom and the olefin unit as potential binding sites (Scheme 1).[24] While a small number of transition and main group metal complexes featuring bidentate dibenzoazepine and -phosphepine ligands

[a] J. Ramler,[+] F. Geist,[+] S. Reith, C. Lichtenberg
Department of Chemistry, Philipps-University Marburg, Hans-Meerwein-Straße 4, 35043 Marburg, Germany
E-mail: crispin.lichtenberg@chemie.uni-marburg.de
[b] C. Mihm, L. Lubczyk
Institute of Inorganic Chemistry, Julius-Maximilians-University Würzburg, Am Hubland, 97074 Würzburg, Germany
[c] C. Herok
Institute of Physical and Theoretical Chemistry, Julius-Maximilians-University Würzburg, Emil-Fischer-Straße 42, 97074 Würzburg, Germany
[d] F. Fantuzzi
School of Chemistry and Forensic Science, University of Kent, Park Wood Rd, Canterbury CT2 7NH, UK
E-mail: f.fantuzzi@kent.ac.uk
[+] These authors contributed equally to this work.
Supporting information for this article is available on the WWW under https://doi.org/10.1002/chem.202403253

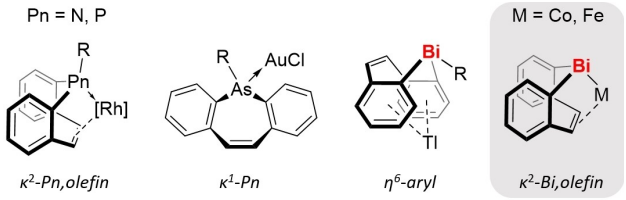

Scheme 1. Selected examples of dibenzoheteropine coordination modes and novel κ^2-*Bi,olefin* coordination mode described in this work.[10,20–22]

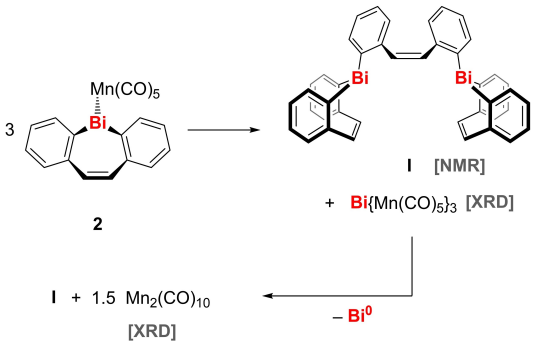

Scheme 3. Suggested decomposition pathway of **2**.

have been reported,[21,22,26] the potential of the heavier arsenic,[27] antimony, and bismuth homologs to complete this intriguing series of bidentate pnictogen/olefin ligands is yet to be demonstrated.

Here we demonstrate that a variety of 3d transition metal bismepinyl species is readily accessible from literature-known starting materials, yielding well-defined molecular complexes featuring the bismepinyl unit in either a monodentate κ^1-*Bi* or in a chelating κ^2-*Bi,olefin* coordination mode, which can be interconverted through photochemical approaches.

Results and Discussion

A range of dibenzobismepine complexes, including a series of halobismepines, a dinuclear bismepine, and cationic bismepines, was recently described by our group,[24] alongside investigations of their soft Lewis acidity[17] and their exploitation as rigid, ditopic arene donor ligands.[10] More recently, we reported on the synthesis of a dibismuthane with two dibenzobismepine units, its reactivity towards chalcogen compounds, and the potential application of the resulting products as hybrid tridentate olefin/chalcogen ligands.[11] Our next goal was to examine the properties of the dibenzobismepinyl group as a ligand in transition metal complexes, especially in view of a possible chelating interaction of the olefinic functionality with transition metal centers.

A salt elimination between the chlorobismepine **1-Cl**[24] and sodium metallates was chosen as the synthetic approach towards bismepinyl-substituted transition metal complexes (Scheme 2). Reaction of **1-Cl** with Na(thf)$_3$[Mn(CO)$_5$] in a mixture of benzene and THF at room temperature led to the formation of [{$C_{14}H_{10}$)Bi{Mn(CO)$_5$}] (**2**), as shown by *in situ* NMR spectroscopy. The ^{1}H and ^{13}C NMR spectra of **2** show the expected signal pattern of the dibenzobismepine unit. The resonances assigned to the olefin unit at 6.92 (^{1}H) and 134.44 (^{13}C) ppm, respectively, are in a similar range as those in halobismepines **1-X** (X = Cl, Br, I),[24] indicating that no bonding interaction between the olefin unit and the manganese center takes place. Due to the facile decomposition of compound **2** (both upon storage in solution and during workup), its isolation and full characterization was not possible. The dinuclear bismepine (**I**), the homoleptic complex [Bi{Mn(CO)$_5$}$_3$] and $Mn_2(CO)_{10}$ were identified as decomposition products by NMR spectroscopy and single crystal X-ray diffraction, respectively. A plausible decomposition pathway is shown in Scheme 3.

The analogous cobalt complex [($C_{14}H_{10}$)Bi{Co(CO)$_4$}] (**3**) was synthesized from **1-Cl** and Na[Co(CO)$_4$] using the same approach. Similar to the literature-known compound [{Ph_2Bi}Co(CO)$_4$], it was only possible to characterize the product in solution due to decomposition during isolation attempts.[28] ^{1}H and ^{13}C NMR spectra are in agreement with the suggested structure. ^{1}H NMR spectroscopic analysis of a solution of **3** in benzene-d_6 revealed a slow and selective conversion (10% after

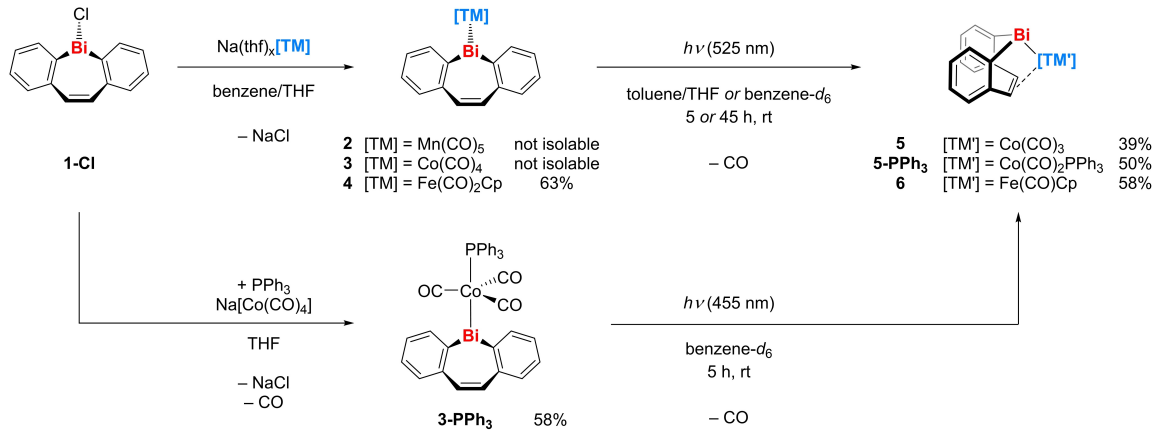

Scheme 2. Synthesis of bismepinyl-substituted transition metal complexes **2**–**6**.

5 h) to a single new species, which was identified as the chelate complex [{κ²*C*,κ¹*Bi*-($C_{14}H_{10}$)Bi}Co(CO)$_3$] (**5**), the selective synthesis and characterization of which will be discussed in a later part of this manuscript. Iron complex [{$C_{14}H_{10}$)Bi{Fe(CO)$_2$Cp}] (**4**) was synthesized according to Scheme 2 at −78 °C and could be isolated in 63% yield as a dark-red solid. The ^{1}H and ^{13}C NMR spectra of compound **4** in benzene-d_6 show the expected signal pattern of the dibenzobismepinyl and cyclopentadienide ligands. When compared to those in manganese complex **2**, the bismepine protons in **4** show a significant downfield shift ($\Delta\delta$ = 0.26–0.86 ppm). The chemical shift of the resonance of the carbonyl ligands in the ^{13}C NMR spectrum (212.49 ppm) is similar to those in [Ph$_2$Bi{Fe(CO)$_2$Cp}] (210.11 ppm)[29] and [{($C_{14}H_{12}$)S}Bi{Fe(CO)$_2$Cp}] (212.03 ppm).[14]

Compound **4** crystallizes in the triclinic space group $P\bar{1}$ with Z = 4 (Figure 1). The asymmetric unit contains two crystallographically distinct molecules, only one of which is discussed herein because the bonding parameters are highly similar. The bismuth center shows a trigonal pyramidal coordination geometry with a C–Bi–C angle of 86.5(3)° and C–Bi–Fe angles of 103.4(2)–105.1(2)°, respectively. These pronounced differences were ascribed to the chelating nature of the diaryl ligand. The iron atom adopts a distorted tetrahedral coordination geometry with angles around Fe1 of 94.9(4)–127.13°. The Bi–Fe bond length of 2.6645(14) Å is similar to previously reported bismuth iron bond lengths.[14,30,31]

Calderazzo *et al.* previously described that exchanging one carbonyl ligand of the non-isolable compound [Co(BiPh$_2$)(CO)$_4$] for triphenyl phosphine (PPh$_3$) significantly stabilizes the resulting complex, which enabled the isolation of [Co(BiPh$_2$)(CO)$_3$(PPh$_3$)].[28] In a similar fashion **3-PPh$_3$** was prepared by reacting **1-Cl** and Na[Co(CO)$_4$] in the presence of one equivalent PPh$_3$ (Scheme 2). **3-PPh$_3$** was isolated in 58% yield as an orange solid. The ^{1}H NMR spectrum shows a doublet for the α-protons (in *ortho*-position to the bismuth substituted carbon atom) at 8.92 ppm, which represents a significant downfield shift when compared to the analogous protons in the previously discussed manganese (**2**; 7.58 ppm) and iron (**4**; 8.13 ppm) complexes. A similar trend has been described for bismuthanyl substituted complexes of the type [{($C_{14}H_{12}$)S}Bi[TM]] with TM = Mn(CO)$_5$, Co(CO)$_3$PPh$_3$, Fe(CO)$_2$Cp.[14] The chemical shift of the resonance assigned to the protons of the olefin unit (6.87 ppm) once again indicates that there is no coordination of the olefin unit to the transition metal center. The ^{13}C NMR spectroscopic resonances of the CO ligands were detected at 201.61 ppm, split into a doublet due to coupling to the adjacent phosphine ligand ($^2J_{PC}$ = 16.3 Hz). The ^{31}P NMR spectrum of **3-PPh$_3$** shows a resonance at 68.22 ppm for the phosphine ligand, which is very close to that in [{($C_{14}H_{12}$)S}Bi{Co(CO)$_3$(PPh$_3$)}] (68.89 ppm).[14] Suitable crystals for X-ray diffraction were obtained by recrystallizing the product from a THF/benzene/*n*–pentane solvent mixture. **3-PPh$_3$** crystallizes in the monoclinic space group $P2_1/c$ with Z = 4 (Figure 2).

Compound **3-PPh$_3$** shows a typical molecular structure in the solid state, directed intermolecular interactions could not be identified based on distance criteria. The cobalt center is found in a trigonal bipyramidal coordination mode (τ_5 = 0.88) with the phosphine and bismepinyl ligands occupying the axial positions. The bismuth center shows a trigonal pyramidal coordination geometry with Bi–C (2.252(3)–2.262(3) Å) and Bi–Co (2.6741(4) Å) bond lengths in the expected ranges.[14,17,24,28]

Compounds **3**, **3-PPh$_3$**, and **4** were additionally characterized by IR spectroscopy. The relevant CO stretching vibrations are summarized in Table 1. The IR spectra show the expected two (**4**), three (**3-PPh$_3$**), or four (**3**) CO stretching vibrations, with

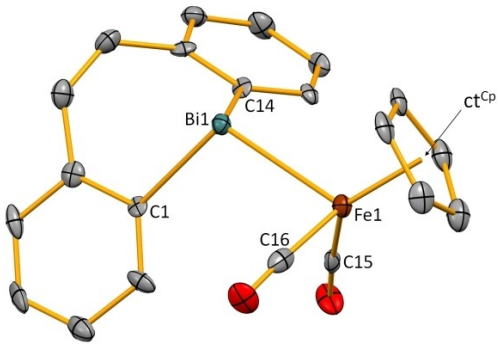

Figure 1. Molecular structure of **4** in the solid state. Displacement ellipsoids are shown at the 50% probability level. Hydrogen atoms are omitted for clarity; ct^{Cp} represents the centroid of the cyclopentadienide ligand. Selected bond lengths (Å) and angles (°): Bi1–C1, 2.262(9); Bi1–C14, 2.259(8); Bi1–Fe1, 2.6644(14); Fe1–C15, 1.754(11); Fe1–C16, 1.772(10); Fe1–ct^{Cp}, 1.717; Fe1–Bi1–C1, 105.1(2); Fe–Bi1–C14, 103.4(2); C1–Bi1–C14, 86.5(3), C16–Fe1–C15, 94.9(4); Bi1–Fe1–ct^{Cp}, 117.75; C15–Fe1–ct^{Cp}, 127.48; C16–Fe1–ct^{Cp}, 127.13.

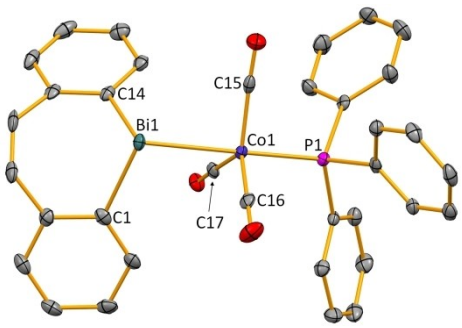

Figure 2. Molecular structure of **3-PPh$_3$** in the solid state. Displacement ellipsoids are shown at the 50% probability level. Hydrogen atoms are omitted for clarity. Selected bond lengths (Å) and angles (°): Bi1–C1, 2.262(3); Bi1–C14, 2.252(3); Bi1–Co1, 2.6741(4); Co1–C15, 1.782(4); Co1–C16, 1.765(4); Co1–C17, 1.783(3); Co1–P1, 2.2045(9); Co1–Bi1–C1, 100.76(9); Co1–Bi1–C14, 99.32(9); C1–Bi1–C14, 89.37(12), C_{CO}–Co1–C_{CO}, 114.93(15)–123.54(15); Bi1–Co1–P1, 176.13(3); C_{CO}–Co1–P1, 91.93(11)–96.91(12).

Table 1.
CO stretching frequencies of compounds **3**, **3-PPh$_3$**, and **4**.

Compound	$\tilde{\nu}_{CO}$ [cm^{-1}]
3[a]	2075, 2036, 2019, 1989
3-PPh$_3$[b]	2010, 1944, 1927
4[b]	1972, 1926

[a] Measured in THF. [b] Measured in substance.

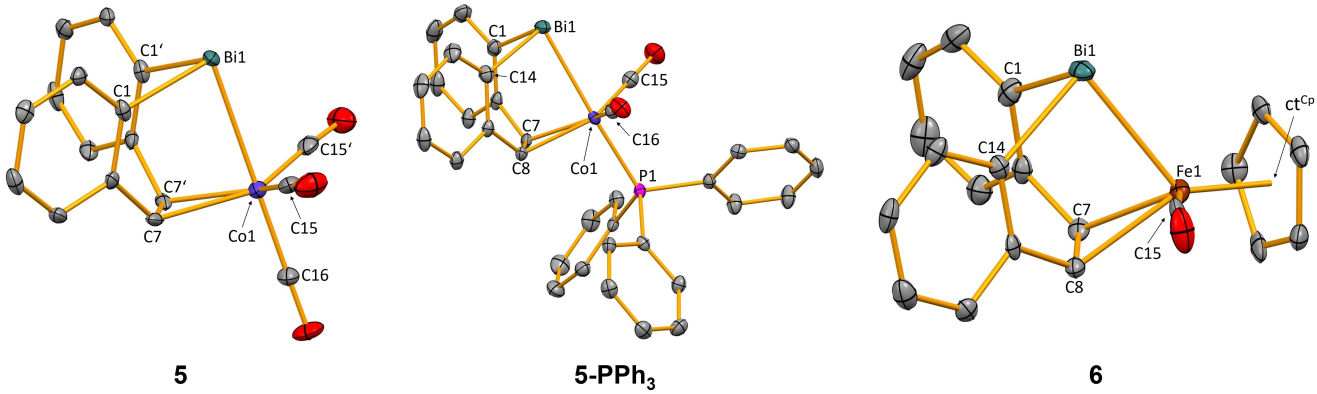

Figure 3. Molecular structures of **5**, **5-PPh$_3$** and **6** in the solid state. Displacement ellipsoids are shown at the 50% probability level. Hydrogen atoms, a second molecule in the asymmetric unit (**5-PPh$_3$**) and one lattice-bound THF molecule (**6**) are omitted for clarity. Selected bonding parameters are summarized in Table 2.

the modes for **3** appearing at higher wavenumbers when compared to those in **3-PPh$_3$**. This is consistent with results from the literature for [(Ph$_2$Bi)Co(CO)$_4$].[28] The number of modes observed and their wavenumber are in agreement with previously obtained results for compounds of the type [{(C$_{14}$H$_{12}$)S}Bi[TM]] (TM = Co(CO)$_3$PPh$_3$, Fe(CO)$_2$Cp).[14]

UV/Vis spectra of compounds **3**, **3-PPh$_3$**, and **4** in THF show absorption maxima at wavelengths of 369 (**3**), 382 (**3-PPh$_3$**), and 362 nm (**4**) respectively, with onsets in the range of 450–510 nm. TD-DFT calculations on compounds **3** and **3-PPh$_3$** revealed that in both cases the first excited states are associated with electron transfer to virtual orbitals featuring Bi–Co and Co–C$_{CO}$/Co–P$_{PPh3}$ σ* contributions, and suggest that the experimental peak at 382 nm for **3-PPh$_3$** is due to charge transfer (CT) excitations from BiL$_2$ to PPh$_3$ (for details, see the Supporting Information, SI). These findings, and the previously mentioned slow conversion (10% after 5 h) of **3** in solution under ambient light, prompted us to investigate the feasibility of a photochemical CO elimination, aiming for the coordination of the dibenzobismepine olefin moiety to the transition metal center.

Irradiation of compounds **3**, **3-PPh$_3$**, and **4** for 5 h (**4**) or 45 h (**3** and **3-PPh$_3$**) with light at wavelengths of 455 nm (**3-PPh$_3$**) or 525 nm (**3**, **4**) led to the formation of compounds **5**, **5-PPh$_3$**, and **6** (Scheme 2). In the case of **5** it was necessary to exchange the atmosphere above the reaction mixture twice during the reaction to achieve complete conversion of starting material **3**, indicating a possible equilibrium between compounds **3** and **5**. The products were isolated in moderate yields (39–58%) as orange (**5**, **5-PPh$_3$**) or dark-red (**6**) solids. ^{1}H NMR spectra of the products show a strong high-field shift ($\Delta\delta$ = 1.61–2.27 ppm) of the resonances assigned to the olefin unit of the bismepinyl ligands in comparison to the starting materials, indicating substantial π(olefin)→metal bonding and metal→π*(olefin) backbonding (also see Figure 3). In the case of **6** all protons of the bismepine backbone are magnetically inequivalent, confirming the chiral-at-metal nature of the tetrahedral iron complex (Figure 4).

The ^{13}C NMR spectra are in agreement with the suggested structures. The ^{31}P NMR resonance of the phosphine ligand in **5-PPh$_3$** is found at 73.94 ppm which corresponds to a downfield shift of 5.72 ppm in comparison to starting material **3-PPh$_3$**. These results indicate the elimination of one carbonyl ligand upon irradiation with simultaneous π-coordination between the olefin functional group and the respective transition metal center. The solid state structures of **5**, **5-PPh$_3$**, and **6** were determined by single-crystal X-ray diffraction analyses (Figure 3).

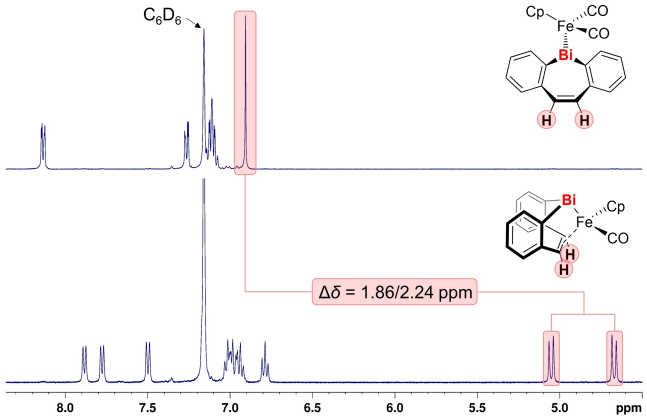

Figure 4. Aromatic region of the ^{1}H NMR spectra of compounds **4** (top) and **6** (bottom) in benzene-d_6. The signals assigned to the protons of the olefin unit of the bismepinyl ligands are highlighted by colored boxes.

5 crystallizes in the orthorhombic space group *Pnma* with Z = 4, **5-PPh$_3$** crystallizes in the triclinic space group $P\bar{1}$ with Z = 4, and **6** crystallizes in the orthorhombic non-centrosymmetric space group $P2_12_12_1$ with Z = 4. Selected bonding parameters are summarized in Table 2. The η^2-coordination mode of the olefin moieties results in the cobalt atoms of **5** and **5-PPh$_3$** adopting (distorted) trigonal bipyramidal coordination geometries with the bismuth atom and one carbonyl ligand (**5**: Bi1–Co1–C$_{trans}$, 179.92(19)°, τ = 0.99) or the phosphane (**5-PPh$_3$**: Bi1–Co1–P1, 173.979(19)°, τ = 0.83) in the axial positions. The bismuth–cobalt bond lengths of ca. 2.69–2.73 Å are slightly longer than that in **3-PPh$_3$**. Reported π-coordinated C–C bond lengths in cobalt complexes are approximately in the range of 1.38–1.41 Å,[32] and are in good agreement with C$_{olefin}$–C$_{olefin}$

Table 2.
Selected bond lengths (Å) and angles (°) of compounds **5**, **5-PPh$_3$**, and **6**.

Bond length/angle	**5**	**5-PPh$_3$**	**6**
Bi–TM	2.7308(9)	2.6904(4)	2.6465(10)
Bi1–C	2.253(4)	2.2250(2), 2.246(2)	2.271(6), 2.258(7)
C_{olefin}–TM	2.083(4)	2.097(2), 2.100(2)	2.137(7), 2.128(7)
C_{olefin}–C_{olefin}	1.371(9)	1.412(3)	1.414(10)
TM–C_{CO}	1.788(5)–1.805(6)	1.765(2)–1.774(2)	1.762(8)
TM–P1/ct^{Cp}	-	2.2442(6)	1.728
C–Bi1–C	83.4(2)	87.58(8)	84.0(2)
C–Bi1–TM	86.16(11)	86.26(6), 86.54(6)	86.71(17), 89.23(16)

bond lengths in **5** (1.371(9) Å), and **5-PPh$_3$** (1.412(3) Å), respectively. The bismuth centers display trigonal pyramidal coordination geometries with Bi–C bond lengths (2.2246(2)–2.253(4) Å) similar to those in previously reported bismepines.[11,17,24] Compared to **3-PPh$_3$** (C–Bi–C: 89.37(12)°; C–Bi–Co: 99.32(9)–100.76(9)), the C–Bi–C/Co angles in **5** and **5-PPh$_3$** are reduced to 83.4(2)–87.58(8)° due to the bite angle of the chelating bonding mode of the bismepinyl ligand. The iron atom in **6** adopts a distorted tetrahedral coordination geometry with angles around the iron atom of 86.71(17)–126.67°. The bismuth atom is found in the expected trigonal pyramidal coordination geometry (C–Bi–C, 84.0(2)°). The olefin functionality occupies the fourth coordination site of the iron atom with a distance of 2.013(7) Å between Fe1 and the center of the C7–C8 bond. The C7–C8 bond in **6** is significantly longer (1.414(10) Å) than in the starting material **4** (1.343(13) Å) and thus in the range of a partial double bond.[33] The Bi–Fe bond length (2.6465(19) Å) is similar to that in **4** (2.6645(14) Å).

The change in the electronic situation of the transition metal atom in complexes **5(-PPh$_3$)** and **6** also shows in their respective CO stretching frequencies. The IR spectra of **5** ($\tilde{\nu}_{CO}$ = 2003 cm^{-1}), **5-PPh$_3$** ($\tilde{\nu}_{CO}$ = 1975, 1923 cm^{-1}) and **6** ($\tilde{\nu}_{CO}$ = 1930 cm^{-1}) show stretching frequencies for the carbonyl ligands at (slightly) lower wavenumbers than the starting materials **3** ($\tilde{\nu}_{CO}$ = 2075–1989 cm^{-1}), **3-PPh$_3$** ($\tilde{\nu}_{CO}$ = 2010–1927 cm^{-1}) and **4** ($\tilde{\nu}_{CO}$ = 1972, 1926 cm^{-1}), suggesting stronger M–CO bonding than in the respective starting materials.

To gain deeper insights into the bonding interactions between the hybrid Bi/olefin ligands and the transition metal (M) centers in **5**, **5-PPh$_3$**, and **6**, these compounds were analyzed by DFT calculations (see the SI). Intrinsic bond orbital (IBO) analyses indicate that the Bi–M bonds in these compounds exhibit a polarized covalent character (Figure 5, top). Specifically, the Bi–Co bonds in **5** and **5-PPh$_3$** are only marginally polarized towards Co with a minimal influence of the ligand in *trans*-position to Bi (CO vs PPh_3). In turn, the covalent Bi–Fe bond in **6** is more strongly polarized towards Bi, demonstrating the tunability of Bi–M bond polarization, depending on the choice of the transition metal complex fragment. Furthermore, the IBO analyses confirm distinct donation of electron density from the olefin to the transition metal (M) and the corresponding M→olefin backdonation, aligning with experimental observations (Figure 5, middle and bottom). Notably, **6** exhibits the highest degree of olefin→M donation, with the M atom contributing 11.0% to the IBO representing this interaction, compared to 4.3% in **5**. In contrast, **5-PPh$_3$** shows enhanced M→olefin backdonation, with the olefin carbon atoms in **5-PPh$_3$** contributing 17.2% to the backdonation IBO, compared to 14.2% in **5**. Correspondingly, the C–C Mayer bond order (MBO) of the olefin decreases in all three systems relative to a bare olefin (formal bond order of 2), with values of 1.29 for **5**, 1.27 for **5-PPh$_3$**, and 1.26 for **6**. These results confirm the significant role of donation and backdonation effects in stabilizing the metal-olefin complexes, consistent with the spectroscopic data.

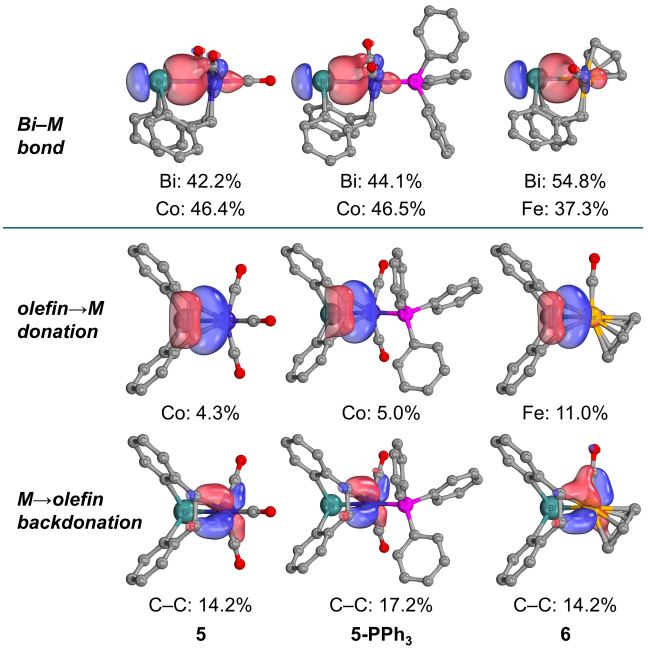

Figure 5. Intrinsic bond orbitals (IBOs) of **5**, **5-PPh$_3$**, and **6** associated with Bi–M bonds (top), olefin→M donation (middle), and M→olefin backdonation (bottom, M = transition metal). The percentages indicate the contribution of the metal atoms and/or the carbon atoms to the IBO representing the covalent Bi–M bond (top), the olefin→M donation (middle), and the M→olefin backdonation (bottom).

The reaction kinetics for the photochemical CO elimination leading to the formation of compounds **5(-PPh$_3$)** and **6** were investigated. ^{1}H NMR spectroscopic reaction monitoring con-

firmed first-order reactions in each case, making more complicated reaction pathways unlikely. Reaction **3** → **5** shows the smallest rate constant, while those associated with **3-PPh$_3$** → **5-PPh$_3$** and **4** → **6** are in a similar range. An overview of the kinetic data is given in Table 3 (for details, see the SI). The relatively slow reaction of compound **3** hints at a more sluggish labilization of a CO ligand in *cis*-position relative to the bismuth atom, which would be necessary for olefin binding without additional isomerization events. Additionally, the redox behavior of the cobalt complexes **3-PPh$_3$**, **5** and **5-PPh$_3$** was investigated by cyclic voltammetry. While the cyclic voltammograms of **3-PPh$_3$** and **5-PPh$_3$** show a complex redox behavior with multiple irreversible oxidation and reduction waves, only one redox wave under oxidative conditions (−0.37 V vs $Fc^{+/0}$) and one redox wave under reducing conditions (−2.17 V vs $Fc^{+/0}$) are present in the cyclic voltammogram of **5**. The chemical reduction of **5** with decamethyl cobaltocene ($CoCp_2^*$) resulted in the reduction of the cobalt carbonyl fragment with formation of $[CoCp_2^*][Co(CO)_4]$ and degradation of the bismepinyl ligand into phenanthrene and elemental bismuth (for more details, see the SI).

The presumed equilibrium between compounds **3** and **5** (*vide supra*) led us to investigate the reversibility of the photochemically induced CO elimination. A high conversion (80%, after 5 h) back to the starting material **3** was observed ^{1}H NMR spectroscopically when CO gas (0.5 bar) was added to a solution of **5** in a C_6D_6/THF-d_8 solvent mixture (5:1). Under the same conditions, the addition of CO to **6** lead to a 1:3 mixture of **4** and **6**, respectively, indicating a partial reversibility of the reaction. The reversibility of the olefin coordination reveals the ability of the bismepinyl unit to act as a hemilabile ligand with a bismuth anchor point, opening up perspectives for potential applications in catalysis.

Table 3.
Overview of the kinetic data of the CO elimination reactions.

Reaction	λ [nm]	Rate constant k [s^{-1}]	$t_{1/2}$ [min]
3 → **5**	455	$(2.04 \pm 0.15) \cdot 10^{-5}$	553
3-PPh$_3$ → **5-PPh$_3$**	525	$(1.98 \pm 0.11) \cdot 10^{-4}$	58
4 → **6**	525	$(2.69 \pm 0.09) \cdot 10^{-4}$	43

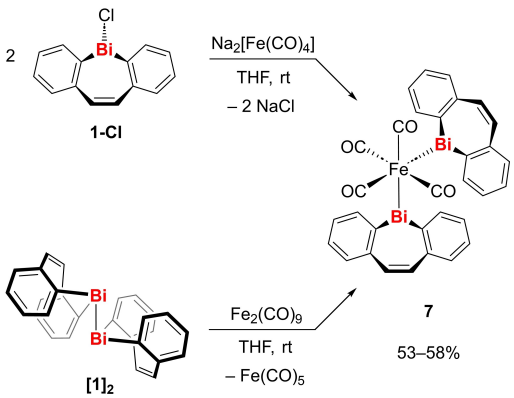

Scheme 4. Synthesis of doubly bismepinyl substituted iron complex **7**.

Based on these results, we became interested in the synthesis and reactivity of doubly bismepinyl substituted transition metal complexes. Analogous to the literature-known synthesis of $[Fe(BiPh_2)_2(CO)_4]$,[30] the iron complex **7** was prepared from **1-Cl** and Collman's reagent ($Na_2[Fe(CO)_4]$) (Scheme 4). Interestingly, the reaction of dibismuthane **[1]$_2$** with $Fe_2(CO)_9$ also afforded **7**, which has previously been hypothesized to represent a potential synthetic access to closely related $[Fe(BiPh_2)_2(CO)_4]$.[30] Compound **7** was isolated in moderate yields (53–58%) as a rust brown solid and fully characterized. ^{1}H and ^{13}C NMR spectra are in agreement with the suggested structure. Suitable crystals for X-ray diffraction analysis were obtained by recrystallization from a toluene/*n*-pentane solvent mixture at −30 °C. **7** crystallizes in the triclinic space group $P\overline{1}$ (Z = 2, Figure 6). The solid state structure shows the two bismepinyl ligands in a *cis*-arrangement, analogous to the parent compound $[Fe(BiPh_2)_2(CO)_4]$.[30] The iron atom adopts the expected octahedral coordination geometry, with a Bi–Fe–Bi angle of 81.66(7)° and C_{CO}–Fe–C_{CO} angles between 94.4(4) and 99.0(4)°. The Bi–Fe bond lengths (2.799(2)/2.7926(19) Å) are longer than those in the previously described iron complexes, presumably due to the steric demand of the two bismepinyl ligands. The distance between the two bismuth atoms in **7** is 3.656(3) Å, which is 12% below the sum of the van-der-Waals radii (4.14 Å).[34] While this suggests the possibility of interactions between the two bismuth atoms, the Bi–Fe–Bi motif is primarily characterized by two Fe–Bi bonds, with only marginal Bi···Bi interactions according to DFT calculations. Specifically, a Mayer bond order of just 0.06 was found for **7**, compared to a value of 0.96 for **[1]$_2$**. Other bond order methods similarly indicated minimal interaction between the Bi atoms, with the largest value being a Wiberg bond index of 0.33 (Table S7). Furthermore, IBO calculations ruled out the existence of a bond, as no IBO orbital involving the Bi centers was identified. Consistently, the quantum theory of atoms in molecules

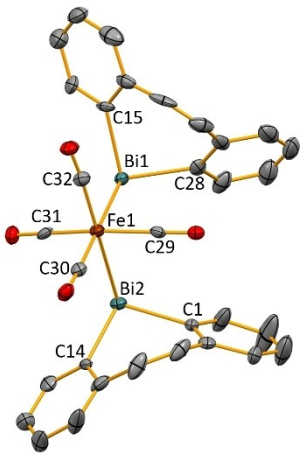

Figure 6. Molecular structure of **7** in the solid state. Displacement ellipsoids are shown at the 50% probability level. Hydrogen atoms are omitted for clarity. Selected bond lengths (Å), interatomic distances (Å) and angles (°): Bi1–C, 2.226(8)–2.237(10); Bi2–C, 2.246(9)–2.263(9); Bi1–Fe1, 2.799(2); Bi2–Fe1, 2.7926(19); Fe1–C_{CO}, 1.801(10)–1.818(9); Bi1···Bi2, 3.656(3); Bi1–Fe1–Bi2, 81.66(7); C1–Bi1–C14, 99.32(9); C–Bi–C, 93.3(4)–94.8(3), C_{CO}–Fe1–C_{CO}, cis: 94.4(4)–99.0(4), trans: 158.4(4).

(QTAIM) analysis revealed no bond critical point between the bismuth atoms (Figure S41). Finally, a relaxed potential energy surface scan of the Bi–Bi internuclear distance from 3.66–2.66 Å revealed the absence of another minimum at shorter bonds, the energy increasing almost 40 kcal/mol during this bond shortening minimum energy path (Figure S42).

The IBO analysis of **7** indicates that each Bi atom has a lone pair in close proximity to one another (Figure S43), suggesting that this bonding motif is induced by the $Fe(CO)_4$ group. Interestingly, a similar proximity-enforced interaction was observed in a bis(germylene) system stabilized by a naphthyridine diimine ligand, recently investigated by some of us.[35] The preference for **7** compared to its *trans*-$[Fe(CO)_4L_2]$ isomer - a configuration that is not observed experimentally - is also supported by our DFT calculations (Figure S44), which indicate that the *trans* isomer is 4.7 kcal/mol higher in energy than **7**. This energy difference is attributed to the stronger *trans* influence exerted by the CO ligand.

The olefin functionalities of the bismepinyl ligands are bent towards the iron center, which could allow CO elimination and the formation of a chelate complex. The IR spectrum of **7** shows four bands for the CO stretching modes at $\tilde{\nu}_{CO} = 2040$, 1981, 1961 and 1933 cm^{-1} which is in a similar range as those in iron complex **4**. The number of modes is in agreement with that expected for a compound of the type *cis*-$[Fe(CO)_4L_2]$. A UV/Vis spectrum of **7** in THF revealed absorption maxima at 288 and 362 nm, with an onset at ca. 450 nm. A solution of **7** in C_6D_6 was irradiated with light at a wavelength of 365 nm and the reaction was monitored by means of ^1H NMR spectroscopy. Under the chosen conditions a decomposition of **7** into dibismuthane $[\mathbf{1}]_2$ (ca. 50% after 2 h, 55% after 4 h) and minor amounts of phenanthrene was observed (Scheme 5). Complete conversion of the starting material could not be achieved by prolonged irradiation, indicating equilibrium conditions.

According to TD-DFT calculations, the broad absorption bands of compound **7**, with maxima at 288 and 362 nm, are associated with depopulation of bonding σ(Bi–Fe) orbitals and the population of an anti-bonding σ*(Bi–Fe) and a bonding σ(Bi–Bi) orbital (see the SI). This is consistent with the formation of $[\mathbf{1}]_2$ from **7**. For the regeneration of compound **7**, photo-activated iron carbonyl species are likely to be involved (see the SI). Without any irradiation, the reaction shown in Scheme 5 also proceeds, albeit much slower. Specifically, a solution of **7** in C_6D_6 released relevant amounts of the dibismuthane $[\mathbf{1}]_2$, when stored under argon atmosphere at ambient temperature and ambient light over prolonged periods of time (18% after 5 d, 52% after 3 months). The formation of minor amounts of a black solid (presumably elemental bismuth) and phenanthrene were also observed, probably due to the even slower decomposition of both bismepine species in solution. These results hint at a possible equilibrium between **7** and dibismuthane $[\mathbf{1}]_2$ plus iron carbonyl species in solution, as proposed in Scheme 5. The addition of CO gas (1 or 5 bar) to a solution of **7** in C_6D_6 did not lead to an accelerated formation of $[\mathbf{1}]_2$, making an associative mechanism unlikely. A mass spectrum (LIFDI) of a solution of **7** in C_6D_6 that was stored for 3 months under argon atmosphere at ambient temperature confirmed the formation of dibismuthane $[\mathbf{1}]_2$ and phenanthrene, however no iron carbonyl species could be identified unambiguously. An IR spectrum of the same solution showed multiple new signals in the expected ranges for stretching vibrations of terminal, as well as bridging, carbonyl ligands, which might be an indication for the formation of multiple iron carbonyl species (i.e. $Fe(CO)_5$, $Fe_2(CO)_9$, $Fe_3(CO)_{12}$, etc.). A partial overlap of these vibrations with those of starting material **7** prohibited a clear assignment of the products. DFT calculations support the feasibility of an equilibrium scenario (see the SI).

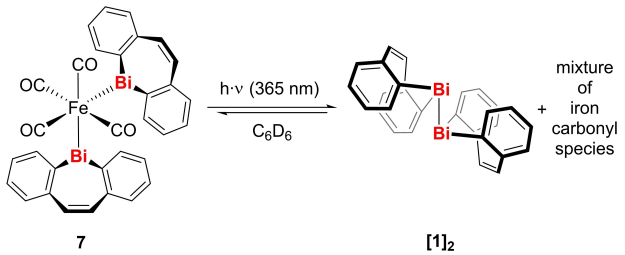

7 $[\mathbf{1}]_2$

Scheme 5. Proposed equilibrium between **7** and $[\mathbf{1}]_2$ + iron carbonyl species.

Conclusion

In conclusion, we have presented the synthesis, isolation, and characterization of a set of transition metal carbonyl complexes with a bismuthanyl ligand, i.e. compounds with a covalent Bi–TM bond (TM = transition metal). These complexes are based on the dibenzo-bismepinyl structural motif with an unsaturated seven-membered bismacycle and bear a free olefin functional group as part of this heterocycle. Olefin coordination can selectively be induced by visible-light-irradiation, with the Bi–TM bond remaining intact. The hybrid bismuth/olefin ligand is hemilabile, as the olefin can be released from the coordination sphere of the transition metal by exposure to an excess of CO. For an iron compound bearing two bismuthanyl ligands, $[Fe(CO)_4(BiR_2)_2]$, we present a peerless equilibrium reaction involving the photochemically induced oxidative addition/reductive elimination of $R_2Bi–BiR_2$. These findings introduce bismepines as soft hybrid bismuth-olefin-ligands, with the potential to be actively engaged in photochemical activation, ligand exchange (by exploiting their hemilabile nature), and oxidative addition/reductive elimination of the corresponding dibismuthane ($R_2Bi–BiR_2$).

Experimental Section

General considerations. All air- and moisture-sensitive manipulations were carried out using standard vacuum line Schlenk techniques or in gloveboxes containing an atmosphere of purified argon. Solvents were degassed and purified according to standard laboratory procedures. Halobismepine **1-Cl** and dibismuthane $[\mathbf{1}]_2$ were prepared according to literature procedures.[11,24] **NMR spectra** were recorded on Bruker instruments operating at 300, 400 or 500 MHz with respect to ^1H. ^1H and ^{13}C NMR chemical shifts are

reported relative to $SiMe_4$ using the residual ^1H and ^{13}C chemical shifts of the solvent as a secondary standard. ^{31}P NMR chemical shifts are reported relative to H_3PO_4 (85% aqueous solution) as an external standard. NMR spectra were recorded at ambient temperature (typically 20 °C), if not otherwise noted. **Elemental analyses** were performed on a Vario Micro Cube by Elementar Analysesysteme GmbH. **UV-vis** measurements were performed under an inert gas atmosphere (glovebox) in quartz glass cuvettes (10 mm) on a UV5 Mettler Toledo UV-vis Excellence or a JASCO-V600 spectrometer. **IR spectra** were recorded either in solution or in pure substance on a JASCO FT/IR-6200 type A spectrometer using a cuvette equipped with a KBr window. **Photochemical experiments** were carried out under a mercury vapor lamp of the type LOT Quantum Design LSB740 (I = 19 A, U = 26 V, 400–500 W) with IR filters irradiating at 210–600 nm, in a MPDSBasic photonCABINET photoreactor from KARLBIEDEN, equipped with photoLAB LED radiation sources of wavelengths 365 (Φe = 43.2 W), 460 (Φe = 26.6–45.0 W), 525 (Φe = 9.0–15.2 W) and 625 nm (Φe = 12.2–20.0 W). thermoCONTROL 100 functions as the cooling unit. All experiments were carried out using borosilicate glassware. Further experiments were carried out with Avance LED lamps (P = 3 W) at wavelength maxima of 400 nm, 455 nm or 525 nm. **Cyclic voltammetry** was performed on a Gamry Instruments Reference [600] potentiostat. For this purpose, a standard three-electrode construction was employed using a platinum disk working electrode, a platinum wire counter electrode, and a silver wire, separated by a Vycor membrane, serving as the reference electrode. The ferrocene/ferrocenium redox couple was used as an internal standard for referencing the measured potential. Tetra-*n*-butylammonium hexafluorophosphate ([nBu$_4$N][PF$_6$], 0.1 M) was used as the electrolyte. Experiments were carried out under an argon atmosphere in a glovebox at ambient temperature. **Crystal data** were collected either on a Bruker Apex II diffractometer with CCD area detector and a multi-mirror monochromator or on a Bruker D8-QUEST diffractometer with CCD area detector and multi-mirror monochromator using MoKα radiation (λ = 0.71073 Å). The respective solid-state structures were solved using intrinsic phase methods (ShelXT), refined with the ShelX software package and developed using Fourier techniques.[36] All non-hydrogen atoms were refined anisotropically. Hydrogen atoms were assigned to idealized positions. The crystallographic data used in the publications were deposited with the Cambridge Crystallographic Data Center (CCDC) and are available at https://www.ccdc.cam.ac.uk/structures with the following CCDC numbers: 2380734 (**3-PPh$_3$**), 2380735 (**4**), 2380736 (**5**), 2380737 (**5-PPh$_3$**), 2380738 (**6**), 2380739 (**7**), 2380740 (**[CoCp$_2$][Co(CO)$_4$]**). The images of the solid-state structures were created with the Mercury software.

The following labeling scheme was used for reporting NMR chemical shifts:

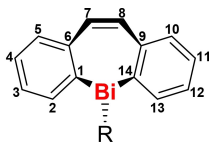

[(C$_{14}$H$_{10}$)Bi{Mn(CO)$_5$}] (2). In a J. Young NMR tube **1-Cl** (15.0 mg, 35.5 μmol) and Na(thf)$_3$[Mn(CO)$_5$] (15.4 mg, 35.5 μmol) were dissolved in benzene-d_6 (0.5 mL). The brown suspension was frozen at 0 °C and after the addition of THF-d_8 (0.1 mL) the suspension was allowed to warm to ambient temperature. Insoluble materials were removed by filtration and the brownish-red filtrate was analyzed by ^1H and ^{13}C NMR spectroscopy, revealing the selective formation of one new species. Isolation of **2** did not succeed due to decomposition during work-up. **^1H NMR** (300 MHz, C$_6$D$_6$/THF-d_8, 5:1): δ = 6.61 (s, 2H, 7,8-CH), 6.97 (ddd, 2H, $^4J_{HH}$ = 1.4 Hz, $^3J_{HH}$ = 7.2 Hz, $^3J_{HH}$ = 7.3 Hz, 4,11-C$_6$H$_4$), 7.07 (ddd, 2H, $^4J_{HH}$ = 1.4 Hz, $^3J_{HH}$ = 7.4 Hz, $^3J_{HH}$ = 7.6 Hz, 3,12-C$_6$H$_4$), 7.27 (dd, 2H, $^4J_{HH}$ = 1.4 Hz, $^3J_{HH}$ = 7.4 Hz, 2,13-C$_6$H$_4$), 7.58 (dd, 2H, $^4J_{HH}$ = 1.4 Hz, $^3J_{HH}$ = 7.3 Hz, 5,10-C$_6$H$_4$) ppm. **^{13}C NMR** (75 MHz, C$_6$D$_6$/THF-d_8, 5:1): δ = 128.06 (s, 3,12-C$_6$H$_4$, overlap with solvent resonance), 128.57 (s, 4,11-C$_6$H$_4$), 133.85 (s, 2,13-C$_6$H$_4$), 134.44 (s, 7,8-CH), 137.63 (s, 5,10-C$_6$H$_4$), 146.20 (s, 6,9-C$_6$H$_4$), 203.99 (s, br, CO) ppm. Note: The ^{13}C resonance for the C-1 and C-14 atoms was neither detected in the ^{13}C NMR spectrum, nor in ^1H, ^{13}C HMBC experiments. This was ascribed to the high quadrupole moment of the ^{209}Bi nucleus (100%, I = 9/2, quadrupole moment $Q = -0.4 \cdot 10^{-28} \cdot m^{-2}$), which broadens the resonances of atoms bonded to the Bi center to such an extent that they may not be observable under standard conditions.

[(C$_{14}$H$_{10}$)Bi{Co(CO)$_4$}] (3). **1-Cl** (15.0 mg, 35.5 μmol) and Na[Co(CO)$_4$] (6.90 mg, 35.5 μmol) were added to a mixture of benzene-d_6 (0.5 mL) and THF-d_8 (0.1 mL). The obtained suspension was filtered. Due to decomposition during work-up, compound **3** was only characterized in solution. **^1H NMR** (500 MHz, C$_6$D$_6$/THF-d_8, 5:1): δ = 6.72 (s, 2H, 7,8-CH), 7.06 (dd, 2H, $^3J_{HH}$ = 7.7 Hz, $^3J_{HH}$ = 7.3 Hz, 4,11-C$_6$H$_4$), 7.20 (d, 2H, $^3J_{HH}$ = 7.5 Hz, 5,10-C$_6$H$_4$), 7.27 (dd, 2H, $^3J_{HH}$ = 7.3 Hz, $^3J_{HH}$ = 7.5 Hz, 3,12-C$_6$H$_4$), 8.47 (d, 2H, $^3J_{HH}$ = 7.7 Hz, 2,13-C$_6$H$_4$) ppm. **^{13}C NMR** (126 MHz, C$_6$D$_6$/THF-d_8, 5:1): δ = 131.17 (s, 3,12-C$_6$H$_4$), 132.25 (s, 7,8-C$_6$H$_4$), 133.10 (s, 5,10-C$_6$H$_4$), 138.66 (s, 4,11-C$_6$H$_4$), 142.43 (s, 2,13-CH), 151.40 (s, 6,9-C$_6$H$_4$), 200.99 (s, CO) ppm. The carbon atoms corresponding to 1,14-C$_6$H$_4$ were not observed in the ^{13}C NMR spectrum due to quadrupole broadening caused by the ^{209}Bi nucleus. **IR (THF):** $\tilde{\nu}_{CO}$ = 2075 (s), 2036 (w), 2019 (s), 1989 (s) cm^{-1}. **UV-vis (THF)**: λ_{max} = 369 nm, onset at 510 nm.

[(C$_{14}$H$_{10}$)Bi{Co(CO)$_3$(PPh$_3$)}] (3-PPh$_3$). A solution of PPh$_3$ (10.6 mg, 0.04 mmol) and Na[Co(CO)$_4$] (7.8 mg, 40.3 μmol) in THF (2.0 mL) was added dropwise to a solution of **1-Cl** (17.0 mg, 40.3 μmol) in THF (1 mL) at −78 °C. After 30 min at −78 °C the reaction mixture was stirred for a further 15 min at ambient temperature. All volatiles were removed under reduced pressure and the residue was extracted with toluene (6 mL) and filtered. The filtrate was layered with *n*-pentane (6 mL). After 3 d at −30 °C **3-PPh$_3$** was isolated by filtration as an orange solid and dried *in vacuo*. **Yield:** 18.4 mg, 22.8 μmol, 58%. **^1H NMR** (400 MHz, C$_6$D$_6$): δ = 6.87 (s, 2H, 7,8-CH), 6.99–7.07 (m, 9H, *para*-PPh$_3$, *meta*-PPh$_3$), 7.09 (ddd, 2H, $^4J_{HH}$ = 1.2 Hz, $^3J_{HH}$ = 7.3 Hz, $^3J_{HH}$ = 7.6 Hz, 4,11-C$_6$H$_4$), 7.24 (d, 2H, $^3J_{HH}$ = 7.6 Hz, 5,10-C$_6$H$_4$), 7.32 (ddd, 2H, $^4J_{HH}$ = 1.2 Hz, $^3J_{HH}$ = 7.3 Hz, $^3J_{HH}$ = 7.9 Hz, 3,12-C$_6$H$_4$), 7.64–7.72 (m, 6H, *ortho*-PPh$_3$), 8.92 (d, 2H, $^3J_{HH}$ = 7.9 Hz, 2,13-C$_6$H$_4$) ppm. **^{13}C NMR** (101 MHz, C$_6$D$_6$): δ = 127.22 (s, 4,11-C$_6$H$_4$), 128.99 (d, $^3J_{PC}$ = 10.2 Hz, *meta*-PPh$_3$), 130.36 (s, 5,10-C$_6$H$_4$), 130.74 (d, $^4J_{PC}$ = 3.0 Hz, *para*-PPh$_3$), 131.45 (s, 3,12-C$_6$H$_4$), 133.55 (d, $^2J_{PC}$ = 11.3 Hz, *ortho*-PPh$_3$), 133.98 (s, 7,8-CH), 135.13 (d, $^1J_{PC}$ = 44.3 Hz, *ipso*-PPh$_3$), 139.54 (s, 2,13-C$_6$H$_4$), 143.36 (s, 6,9-C$_6$H$_4$), 145.38 (s, br, 1,14-C$_6$H$_4$) 201.61 (d, $^2J_{PC}$ = 16.9 Hz, CO) ppm. **^{31}P NMR** (121 MHz, C$_6$D$_6$): δ = 68.22 (s, PPh$_3$) ppm. **IR (neat):** $\tilde{\nu}_{CO}$ = 1927 (s), 1944 (s), 2010 (w) cm^{-1}. **UV-vis (THF):** λ_{max} = 382 nm, onset at 480 nm. **Elemental analysis:** Anal. calc. (%) for C$_{35}$H$_{25}$BiCoO$_3$P (792.47 g · mol^{-1}): C 53.05, H 3.18; found: C 53.05, H 3.09.

[(C$_{14}$H$_{10}$)Bi{Fe(CO)$_2$Cp}] (4). A solution of Na(thf)[FeCp(CO)$_2$] (35.6 mg, 130 μmol) in THF (2.5 ml) was added to a solution of **1-Cl** (54.9 mg, 130 μmol) in THF (2.5 ml) at −78 °C in small portions. After stirring for 30 min at −78 °C the reaction mixture was allowed to warm up to ambient temperature and stirred for a further 30 min. All volatiles were removed under reduced pressure and the residue was extracted with toluene (6 mL) and filtered. The filtrate was layered with *n*-pentane (7 mL). After 3 d at −30 °C **4** was obtained as a dark red solid by filtration and dried *in vacuo*. **Yield**: 46.0 mg, 80.0 μmol, 63%. **^1H NMR** (400 MHz, C$_6$D$_6$): δ = 4.06 (s, 5H, Cp), 6.91 (s, 2H, 7,8-CH), 7.09–7.13 (m, 4H, 3,12-C$_6$H$_4$, 4,11-C$_6$H$_4$), 7.25–7.28 (m, 2H, 5,10-C$_6$H$_4$), 8.13 (dd, 2H, $^4J_{HH}$ = 1.8 Hz, $^3J_{HH}$ = 7.1 Hz, 2,13-C$_6$H$_4$) ppm. **^{13}C NMR** (101 MHz, C$_6$D$_6$): δ = 83.30 (s, Cp), 127.30

(s, 4,11-C_6H_4), 129.72 (s, 3,12-C_6H_4), 130.65 (s, 5,10-C_6H_4), 134.56 (s, 7,8-CH), 135.41 (s, br, 1,14-C_6H_4), 139.04 (s, 2,13-C_6H_4), 144.72 (s, 6,9-C_6H_4), 212.49 (s, CO) ppm. **IR (neat):** $\tilde{\nu}_{CO}$ = 1972 (s), 1926 (s) cm^{-1}. **UV-vis (THF):** λ_{max} = 362 nm, onset at 450 nm. **Elemental analysis**: Anal. calc. (%) for $C_{21}H_{15}BiFeO_2$ (564.17 g · mol^{-1}): C 44.71, H 2.68; found: C 45.10, H 2.73.

[{κ²*C*,κ¹*Bi*-($C_{14}H_{10}$)Bi}Co(CO)₃] (5). A suspension of **1-Cl** (20.0 mg, 47.3 μmol) and Na[$Co(CO)_4$] (9.20 mg, 47.3 μmol) in a mixture of toluene/THF (0.7 mL, 1:0.05) was irradiated (525 nm) for 45 h. The suspension was filtered and the filtrate was layered with *n*-pentane (1.5 mL). After 16 h at −30 °C **5** was obtained by filtration and dried *in vacuo*. **Yield:** 10.0 mg, 18.3 μmol, 39 %. **^{1}H NMR** (500 MHz, C_6D_6): δ = 5.11 (s, 2H, 7,8-CH_2), 6.95 (m, 4H, 3,12-C_6H_4, 4,11-C_6H_4), 7.31 (d, 2H, $^3J_{HH}$ = 7.5 Hz, 5,10-C_6H_4), 7.39 (d, 2H, $^3J_{HH}$ = 7.1 Hz, 2,13-C_6H_4) ppm. **^{13}C NMR** (126 MHz, C_6D_6): δ = 75.60 (s, 7,8-CH), 126.50 (s, 4,11-C_6H_4), 127.55 (s, 3,12-C_6H_4), 131.64 (s, 5,10-C_6H_4), 134.08 (s, 2,13-C_6H_4), 147.66 (s, br, 1,14-C_6H_4), 154.64 (s, 6,9-C_6H_4), 207.00 (s, br, CO) ppm. **IR (neat):** $\tilde{\nu}_{CO}$ = 2003 (s) cm^{-1}. **UV-vis (THF):** λ_{max} = 346 nm, onset at 420 nm. **Elemental analysis**: Anal. calc. (%) for $C_{17}H_{10}O_3CoBi$ (530.17 g · mol^{-1}): C 38.51, H 1.90; found: C 38.41, H 2.05.

[{κ²*C*,κ¹*Bi*-($C_{14}H_{10}$)Bi}Co(CO)₂(PPh_3)] (5-PPh_3). A solution of **3-PPh_3** (34.8 mg, 40.0 μmol) in benzene-d_6 was irradiated (455 nm) for 5 h. Small amounts of a black, insoluble precipitate were removed by filtration and the yellow filtrate was layered with *n*-pentane (2 mL) and stored at ambient temperature. After 16 h **5-PPh_3** was isolated as an orange solid by filtration and dried *in vacuo*. **Yield:** 16.3 mg, 20.0 μmol, 50 %. **^{1}H NMR** (300 MHz, C_6D_6): δ = 4.60 (d, 2H, $^3J_{HP}$ = 7.0 Hz, 7,8-CH), 6.94–7.01 (m, 13H, *para*-PPh_3, 3,12-C_6H_4, 4,11-C_6H_4, *meta*-PPh_3), 7.33–7.36 (m, 2H, 5,10-C_6H_4), 7.59–7.66 (m, 6H, *ortho*-PPh_3), 7.70–7.73 (m, 2H, 2,13-C_6H_4) ppm. **^{13}C NMR** (126 MHz, C_6D_6): δ = 76.24 (s, 7,8-CH), 126.35 (d, $^4J_{PC}$ = 12.1 Hz, 4,11-C_6H_4), 128.62 (s, 3,12-C_6H_4) 128.94 (d, $^3J_{PC}$ = 9.4 Hz, *meta*-PPh_3), 130.18 (s, 5,10-C_6H_4), 130.51 (d, $^4J_{PC}$ = 2.2 Hz, *para*-PPh_3), 133.51 (s, 2,13-C_6H_4), 133.94 (d, $^2J_{PC}$ = 10.7 Hz, *ortho*-PPh_3), 135.09 (d, $^1J_{PC}$ = 1.2 Hz, *ipso*-PPh_3), 143.11 (s, br, 1,14-C_6H_4), 156.79 (d, $^3J_{PC}$ = 5.7 Hz, 6,9-C_6H_4), 205.15 (s, br, CO) ppm. **^{31}P NMR** (121 MHz, C_6D_6): δ = 73.94 (s) ppm. **IR (neat)**: $\tilde{\nu}_{CO}$ = 1975 (s), 1923 (s) cm^{-1}. **UV-vis (THF):** λ_{max} = 360 nm, 435 nm. **Elemental analysis:** Anal. calc. (%) for $H_{25}CoBiC_{34}O_2P$ (764.45 g · mol^{-1}): C 53.42, H 3.30; found: C 53.71, H 3.34.

[{κ²*C*,κ¹*Bi*-($C_{14}H_{10}$)Bi}Fe(CO)Cp] (6). A solution of **4** (20.0 mg, 34.5 μmol) in benzene-d_6 (0.5 mL) was irradiated (525 nm) for 5 h. Small amounts of black, insoluble solid were removed by filtration and the obtained dark red solution was layered with *n*-pentane (1 mL). After 16 h at −30 °C **6** was obtained as a dark red, crystalline solid by filtration and dried *in vacuo*. **Yield:** 11.0 mg, 19.9 μmol, 58 %. **^{1}H NMR** (400 MHz, C_6D_6): δ = 3.88 (s, 5H, Cp), 4.66 (d, 1H, $^3J_{HH}$ = 10.5 Hz, 7-CH), 5.03 (d, 1H, $^3J_{HH}$ = 10.5 Hz, 8-CH), 6.77 (dd, 1H, $^3J_{HH}$ = 7.2 Hz, $^3J_{HH}$ = 7.3 Hz, 12-C_6H_4), 6.75–7.00 (m, 3H, 3-C_6H_4, 4,11-C_6H_4), 7.16 (m, 1H, 5-C_6H_4, overlap with solvent signal), 7.48 (d, 1H, $^3J_{HH}$ = 7.6 Hz, 10-C_6H_4), 7.76 (d, 1H, $^3J_{HH}$ = 7.2 Hz, 13-C_6H_4), 7.87 (d, 1H, $^3J_{HH}$ = 7.3 Hz, 2-C_6H_4) ppm. **^{13}C NMR** (101 MHz, C_6D_6): δ = 69.66 (s, 7-CH), 73.53 (s, 8-CH), 81.30 (s, Cp), 125.27 (s, 4-C_6H_4), 125.85 (s, 12-C_6H_4), 126.00 (s, 3-C_6H_4), 126.29 (s, 11-C_6H_4), 128.73 (s, 10-C_6H_4), 130.31 (s, br, 1-C_6H_4), 132.08 (s, 5-C_6H_4), 132.48 (s, br, 14-C_6H_4) 135.41 (s, 2-C_6H_4), 137.00 (s, 13-C_6H_4), 153.34 (s, 6-C_6H_4), 158.43 (s, 9-C_6H_4), 220.22 (s, CO) ppm. **IR (neat):** $\tilde{\nu}_{CO}$ = 1930 (s) cm^{-1}. **UV-vis (THF)**: λ_{max} = 353 nm. **Elemental analysis:** Anal. calc. (%) for $C_{20}H_{15}BiFeO$ (536.16 g · mol^{-1}): C 44.80, H 2.82; found: C 44.60, H 2.71.

[{($C_{14}H_{10}$)Bi}₂Fe(CO)₄] (7). *Route A:* A suspension of $Na_2Fe(CO)_4$ (5.1 mg, 23.7 μmol) in THF (2 mL) was added dropwise to a solution of chloro-bismepine **1-Cl** (20.0 mg, 47.4 μmol) in THF (2 mL). The reaction mixture was stirred for 2 h at ambient temperature, after which all volatiles were removed under reduced pressure. The residue was extracted with toluene (3×1 mL) and filtered. The filtrate was layered with *n*-pentane and stored at −30 °C. After 16 h **7** was isolated as a red, crystalline solid by filtration and dried *in vacuo*. **Yield:** 11.8 mg, 12.5 μmol, 53 %.

Route B: $Fe_2(CO)_9$ (14.0 mg, 39.0 μmol) was added to a solution of dibismuthane **[1]₂** (30.0 mg, 38.7 μmol) in THF (6 mL). The reaction mixture was stirred for 1 d at ambient temperature, after which all volatiles were removed under reduced pressure. The residue was extracted with toluene (3×2 mL) and filtered. The filtrate was layered with *n*-pentane (6 mL) and stored at −30 °C. After 16 h **7** was isolated as a red solid by filtration, washed with *n*-pentane (4 mL) and dried *in vacuo*. Yield: 21.0 mg, 22.3 μmol, 58 %. When $Fe(CO)_5$ was added to solutions of **[1]₂** in THF-d_8 or benzene-d_6, the slow and selective formation of **7** was observed via ^{1}H NMR spectroscopy, however full conversion of the starting material could not be achieved (even when an excess of $Fe(CO)_5$ was used) and the reaction proceeded at a lower rate than that with $Fe_2(CO)_9$ as the Fe precursor.

^{1}H NMR (500 MHz, C_6D_6): δ = 6.66 (s, 4H, 7,8-C_2H_2), 7.00 (ddd, 4H, $^3J_{HH}$ = 7.3 Hz, $^3J_{HH}$ = 7.3 Hz, $^4J_{HH}$ = 1.4 Hz, 3,12-C_6H_4), 7.06 (ddd, 4H, $^3J_{HH}$ = 7.5 Hz, $^3J_{HH}$ = 7.5 Hz, $^4J_{HH}$ = 1.5 Hz, 4,11-C_6H_4), 7.30 (dd, 4H, $^3J_{HH}$ = 7.7 Hz, $^4J_{HH}$ = 1.3 Hz, 5,10-C_6H_4), 7.56 (dd, 4H, $^3J_{HH}$ = 7.3 Hz, $^4J_{HH}$ = 1.4 Hz, 2,13-C_6H_4) ppm. **^{13}C NMR** (126 MHz, C_6D_6): δ = 128.53 (s, 3,12-C_6H_4), 128.60 (s, 4,11-C_6H_4), 133.99 (s, 5,10-C_6H_4), 134.34 (s, 7,8-C_6H_4), 137.44 (s, 2,13-C_2H_2), 143.93 (s, 1,14-C_6H_4), 146.09 (s, 6,9-C_6H_4) ppm. The signal for the carbon atoms of the CO ligands could not be detected. **IR (neat):** $\tilde{\nu}_{CO}$ = 2040 (s), 1981 (w), 1961 (s), 1933 (w) cm^{-1}. **UV-vis (THF):** λ_{max} = 362 nm, onset at ca. 450 nm. **Elemental analysis**: Anal. calc. (%) for $C_{32}H_{20}Bi_2FeO_4$ (942.31 g · mol^{-1}): C 40.79, H 2.14; found: C 40.92, H 2.19.

Computational Details. Geometry optimizations and vibrational frequency calculations were carried out at the B3LYP[37]-D3(BJ)[38]/bs1 level of theory, where bs1 consists of def2-TZVP for Co and Fe, def2-SVPD for Bi and P, def2-ECP for Bi core electrons, and def2-SVP for the remaining atoms.[39] All calculated systems in this work are confirmed as minimum energy structures, as evidenced by the presence of only real vibrational frequencies and positive eigenvalues across all modes. The resolution of the identity Coulomb (RI-J) method, combined with the chain-of-spheres exchange (COSX) approximation, known as the RIJCOSX method, was employed to speed up the calculations.[40] The bonding situation of complex **7** was analyzed using multiple bond analysis methods available in Multiwfn 3.8,[41] including Mayer bond order,[42] Wiberg bond order,[43] Mulliken bond order,[44] fuzzy bond order,[45] Laplacian bond order,[46] and intrinsic bond strength index.[47] Additionally, the intrinsic bond orbital (IBO)[48] method was employed to further evaluate bonding interactions. Vertical electronic excitations for compounds **[1]₂**, **3**, **3-PPh_3**, and **7** were computed using TD-DFT at the CAM-B3LYP[49]-D3(BJ)/bs2 level of theory. These calculations were performed without the Tamm–Dancoff approximation. The basis set bs2 includes def2-TZVP for Co and Fe, def2-SVPD for the remaining atoms, and def2-ECP for Bi core electrons. This level of theory was also applied in the relaxed scan calculations to track the dissociation of the Bi–Bi bond in **[1]₂**. All (TD-)DFT calculations were performed in ORCA 5.0.3.[50] Charge density differences (CDDs) and the charge transfer (CT) character of the electronic excitations were analyzed using Multiwfn 3.8, with the CT analysis carried out via the interfragment charge transfer method as implemented in the software. Additionally, natural transition orbitals (NTOs)[51] were generated to further characterize the nature of the electronic transitions. The NTO calculations were performed using the TheoDORE program.[52] All transitions discussed correspond to singlet-singlet excitations. Finally, reaction enthalpies and free energies were computed at the ωB97X-D3[53]/bs2 from optimized

structures at the B3LYP-D3(BJ)/bs1. Solvent corrections were included using the conductor-like polarizable continuum model (CPCM)[54] and benzene ($\varepsilon = 2.28$) as the solvent. To accurately account for associative and dissociative steps, a concentration correction of $\Delta G^{0\rightarrow *} = 1.89$ kcal/mol was applied to the free energy values of all calculated species, adjusting for the change in standard state from the gas phase (1 atm) to the condensed phase (1 M).[55]

Acknowledgements

Funding through the DFG (LI 2860/5-1) and the LOEWE program (LOEWE/4b//519/05/01.002(0002)/85) is gratefully acknowledged. This project has received funding from the European Research Council (ERC) under the European Union's Horizon 2020 research and innovation program (grant agreement No 946184). F. F. acknowledges the financial and computational support provided by the University of Kent and Julius-Maximilians-Universität Würzburg. This article is also based upon work from the COST Action CA20129 - Multiscale Irradiation and Chemistry Driven Processes and Related Technologies (MultIChem), supported by COST (European Cooperation in Science and Technology). Open Access funding enabled and organized by Projekt DEAL.

Conflict of Interest

The authors declare no conflict of interest.

Keywords: Bismuth · Bismuth transition metal complexes · Carbonyl ligands · Dibismuthanes · Olefin ligands

[1] V. K. Greenacre, W. Levason, G. Reid, *Coord. Chem. Rev.* **2021**, *432*, 213698.
[2] S. L. Benjamin, G. Reid, *Coord. Chem. Rev.* **2015**, *297–298*, 168–180.
[3] N. R. Champness, W. Levason, *Coord. Chem. Rev.* **1994**, *133*, 115–217.
[4] S. Roggan, C. Limberg, *Inorg. Chim. Acta* **2006**, *359*, 4698–4722.
[5] H. Braunschweig, P. Cogswell, K. Schwab, *Coord. Chem. Rev.* **2011**, *255*, 101–117.
[6] K. H. Whitmire, *J. Clust. Sci.* **1991**, *2*, 231–258.
[7] J. Ramler, C. Lichtenberg, *Dalton Trans.* **2021**, *50*, 7120–7138.
[8] a) C. Tschersich, S. Hoof, N. Frank, C. Herwig, C. Limberg, *Inorg. Chem.* **2016**, *55*, 1837–1842; b) C. Tschersich, C. Limberg, S. Roggan, C. Herwig, N. Ernsting, S. Kovalenko, S. Mebs, *Angew. Chem. Int. Ed.* **2012**, *51*, 4989–4992; c) T.-P. Lin, I.-S. Ke, F. P. Gabbaï, *Angew. Chem. Int. Ed.* **2012**, *51*, 4985–4988; d) C. Tschersich, B. Braun, C. Herwig, C. Limberg, *Organometallics* **2015**, *34*, 3782–3787; e) J. Ramler, K. Radacki, J. Abbenseth, C. Lichtenberg, *Dalton Trans.* **2020**, *49*, 9024–9034.
[9] D. Meleschko, P. Palui, R. M. Gomila, G. Schnakenburg, A. C. Filippou, A. Frontera, A. Bismuto, *Angew. Chem. Int. Ed.* **2024**, *63*,e202405400.
[10] J. Ramler, L. Wüst, A. Rempel, L. Wolz, C. Lichtenberg, *Organometallics* **2021**, *40*, 832–837.
[11] F. Geist, S. Martínez, J. Ramler, K. Oberdorf, L. Brändler, S. Reith, C. Lichtenberg, *Eur. J. Inorg. Chem.* **2023**, *26*, e202300415.
[12] a) A. J. Plajer, A. L. Colebatch, F. J. Rizzuto, P. Pröhm, A. D. Bond, R. García-Rodríguez, D. S. Wright, *Angew. Chem. Int. Ed.* **2018**, *57*, 6648–6652; b) Á. García-Romero, J. E. Waters, R. B. Jethwa, A. D. Bond, A. L. Colebatch, R. García-Rodríguez, D. S. Wright, *Inorg. Chem.* **2023**, *62*, 4625–4636; c) J. E. Waters, G. Berger, A. J. Peel, R. García-Rodríguez, A. D. Bond, D. S. Wright, *Chem. Eur. J.* **2021**, *27*, 12036–12040.
[13] A. Stoy, M. Jürgensen, C. Millidoni, C. Berthold, J. Ramler, S. Martínez, M. R. Buchner, C. Lichtenberg, *Angew. Chem. Int. Ed.* **2023**, *62*, e202308293.
[14] J. Ramler, I. Krummenacher, C. Lichtenberg, *Angew. Chem. Int. Ed.* **2019**, *58*, 12924–12929.
[15] J. Ramler, F. Fantuzzi, F. Geist, A. Hanft, H. Braunschweig, B. Engels, C. Lichtenberg, *Angew. Chem. Int. Ed.* **2021**, *60*, 24388–24394.
[16] K. Materne, B. Braun-Cula, C. Herwig, N. Frank, C. Limberg, *Chem. Eur. J.* **2017**, *23*, 11797–11801.
[17] J. Ramler, C. Lichtenberg, *Chem. Eur. J.* **2020**, *26*, 10250–10258.
[18] a) C. Lichtenberg, *Advances in Inorganic Chemistry : Inorganic Chemistry in Germany* (Eds: K. Meyer, R. van Eldik), Academic Press, Cambridge **2023**, pp. 237–260; b) S. S. Garje, V. K. Jain, *Main Group Met. Chem.* **1999**, *22*, 45–58; c) T.-L. Ho, *Chem. Rev.* **1975**, *75*, 1–20.
[19] a) C. Defieber, H. Grützmacher, E. M. Carreira, *Angew. Chem. Int. Ed.* **2008**, *47*, 4482–4502; b) F. Läng, F. Breher, D. Stein, H. Grützmacher, *Organometallics* **2005**, *24*, 2997–3007; c) C. Lichtenberg, L. Viciu, M. Adelhardt, J. Sutter, K. Meyer, B. de Bruin, H. Grützmacher, *Angew. Chem. Int. Ed.* **2015**, *54*, 5766–5771; d) C. Lichtenberg, I. Garcia Rubio, L. Viciu, M. Adelhardt, K. Meyer, G. Jeschke, H. Grützmacher, *Angew. Chem. Int. Ed.* **2015**, *54*, 13012–13017; e) C. Lichtenberg, L. Viciu, M. Vogt, R. E. Rodríguez-Lugo, M. Adelhardt, J. Sutter, M. M. Khusniyarov, K. Meyer, B. de Bruin, E. Bill, H. Grützmacher, *Chem. Commun.* **2015**, *51*, 13890–13893; f) C. Lichtenberg, M. Adelhardt, T. L. Gianetti, K. Meyer, B. de Bruin, H. Grützmacher, *ACS Catal.* **2015**, *5*, 6230–6240; g) T. Büttner, J. Geier, G. Frison, J. Harmer, C. Calle, A. Schweiger, H. Schönberg, H. Grützmacher, *Science* **2005**, *307*, 235–238; h) M. Vogt, B. de Bruin, H. Berke, M. Trincado, H. Grützmacher, *Chem. Sci.* **2011**, *2*, 723; i) Y. Li, M.-H. Xu, *Chem. Commun.* **2014**, *50*, 3771–3782; j) W.-L. Duan, H. Iwamura, R. Shintani, T. Hayashi, *J. Am. Chem. Soc.* **2007**, *129*, 2130–2138.
[20] I. Kawashima, H. Imoto, M. Ishida, H. Furuta, S. Yamamoto, M. Mitsuishi, S. Tanaka, T. Fujii, K. Naka, *Angew. Chem. Int. Ed.* **2019**, *58*, 11686–11690.
[21] V. Lyaskovskyy, R. J. A. van Dijk-Moes, S. Burck, W. I. Dzik, M. Lutz, A. W. Ehlers, J. C. Slootweg, B. de Bruin, K. Lammertsma, *Organometallics* **2013**, *32*, 363–373.
[22] I. Heuermann, B. Heitmann, R. Stichauer, D. Duvinage, M. Vogt, *Organometallics* **2019**, *38*, 1787–1799.
[23] S. Yasuike, H. Ohta, S. Shiratori, J. Kurita, T. Tsuchiya, *J. Chem. Soc., Chem. Commun.* **1993**, 1817.
[24] J. Ramler, K. Hofmann, C. Lichtenberg, *Inorg. Chem.* **2020**, *59*, 3367–3376.
[25] A small number of bismepines has been reported that do not fall into the category of dibenzobismepines: a) S. Yasuike, T. Kiharada, J. Kurita, T. Tsuchiya, *Chem. Commun.* **1996**, 2183–2184; b) S. Yasuike, F. Nakashima, J. Kurita, T. Tsuchiya, *Heterocycles* **1997**, *45*, 1899–1902.
[26] a) B. Freitag, H. Elsen, J. Pahl, G. Ballmann, A. Herrera, R. Dorta, S. Harder, *Organometallics* **2017**, *36*, 1860–1866; b) W. Winter, J. Strähle, *Angew. Chem. Int. Ed.* **1978**, *17*, 128–129; c) J. Campos, J. López Serrano, E. Álvarez, E. Carmona, *J. Am. Chem. Soc.* **2012**, *134*, 7165–7175.
[27] A gold complex of dibenzoarsepine has been reported, but the gold atom interacts only with the arsenic atom, not the the olefin unit: I. Kawashima, H. Imoto, M. Ishida, H. Furuta, S. Yamamoto, *Angew. Chem. Int. Ed.* **2019**, *58*, 11686–11690.
[28] F. Calderazzo, R. Poli, G. Pelizzi, *J. Chem. Soc., Dalton Trans.* **1984**, 2535.
[29] The synthesis of this compound is described in chapter I of the Supporting Information.
[30] J. M. Cassidy, K. H. Whitmire, *Inorg. Chem.* **1991**, *30*, 2788–2795.
[31] L. Balzs, H. J. Breunig, E. Lork, *Z. Anorg. Allg. Chem.* **2004**, *630*, 1937–1940.
[32] a) C. Chen, T. R. Dugan, W. W. Brennessel, D. J. Weix, P. L. Holland, *J. Am. Chem. Soc.* **2014**, *136*, 945–955; b) A. Gutnov, H.-J. Drexler, A. Spannenberg, G. Oehme, B. Heller, *Organometallics* **2004**, *23*, 1002–1009; c) I. Thiel, M. Lamač, H. Jiao, A. Spannenberg, M. Hapke, *Organometallics* **2013**, *32*, 3415–3418.
[33] M. A. Fox, J. K. Whitesell, *Organische Chemie*, Akademischer Verlag, Heidelberg **1995**.
[34] M. Mantina, A. C. Chamberlin, R. Valero, C. J. Cramer, D. G. Truhlar, *J. Phys. Chem. A* **2009**, *113*, 5806–5812.
[35] a) J. Cui, J. Weiser, F. Fantuzzi, M. Dietz, Y. Yatsenko, A. Häfner, S. Nees, I. Krummenacher, M. Zhang, K. Hammond, P. Roth, W. Lu, R. D. Dewhurst, B. Engels, H. Braunschweig, *Chem. Commun.* **2022**, *58*, 13357–13360; b) J. Weiser, J. Cui, R. D. Dewhurst, H. Braunschweig, B. Engels, F. Fantuzzi, *J. Comput. Chem.* **2023**, *44*, 456–467.

[36] a) G. Sheldrick, *Acta Cryst. A* **2014**, *70*, C1437–C1437; b) G. M. Sheldrick, *Acta Cryst. A* **2008**, *64*, 112–122; c) G. M. Sheldrick, *Acta Cryst. A* **2015**, *71*, 3–8.
[37] a) S. H. Vosko, L. Wilk, M. Nusair, *Can. J. Phys.* **1980**, *58*, 1200–1211; b) C. Lee, W. Yang, R. G. Parr, *Phys. Rev. B Condens.* **1988**, *37*, 785–789; c) A. D. Becke, *J. Chem. Phys.* **1993**, *98*, 5648–5652; d) P. J. Stephens, F. J. Devlin, C. F. Chabalowski, M. J. Frisch, *J. Phys. Chem.* **1994**, *98*, 11623–11627.
[38] a) S. Grimme, J. Antony, S. Ehrlich, H. Krieg, *J. Chem. Phys.* **2010**, *132*, 154104; b) S. Grimme, S. Ehrlich, L. Goerigk, *J. Comput. Chem.* **2011**, *32*, 1456–1465.
[39] a) B. Metz, H. Stoll, M. Dolg, *J. Chem. Phys.* **2000**, *113*, 2563–2569; b) F. Weigend, R. Ahlrichs, *Phys. Chem. Chem. Phys.* **2005**, *7*, 3297–3305.
[40] a) F. Neese, *J. Comput. Chem.* **2003**, *24*, 1740–1747; b) F. Neese, F. Wennmohs, A. Hansen, U. Becker, *Chem. Phys.* **2009**, *356*, 98–109.
[41] T. Lu, F. Chen, *J. Comput. Chem.* **2012**, *33*, 580–592.
[42] I. Mayer, *Int. J. Quantum Chem.* **1984**, *26*, 151–154.
[43] K. B. Wiberg, *Tetrahedron* **1968**, *24*, 1083–1096.
[44] R. S. Mulliken, *J. Chem. Phys.* **1955**, *23*, 1833–1840.
[45] I. Mayer, P. Salvador, *Chem. Phys. Lett.* **2004**, *383*, 368–375.
[46] T. Lu, F. Chen, *J. Phys. Chem. A* **2013**, *117*, 3100–3108.
[47] J. Klein, H. Khartabil, J.-C. Boisson, J. Contreras-García, J.-P. Piquemal, E. Hénon, *J. Phys. Chem. A* **2020**, *124*, 1850–1860.
[48] G. Knizia, *J. Chem. Theory Comput.* **2013**, *9*, 4834–4843.
[49] T. Yanai, D. P. Tew, N. C. Handy, *Chem. Phys. Lett.* **2004**, *393*, 51–57.
[50] F. Neese, *WIREs Comput Mol Sci.* **2022**, *12*, e1606.
[51] R. L. Martin, *J. Chem. Phys.* **2003**, *118*, 4775–4777.
[52] F. Plasser, *J. Chem. Phys.* **2020**, *152*, 84108.
[53] Y.-S. Lin, G.-D. Li, S.-P. Mao, J.-D. Chai, *J. Chem. Theory Comput.* **2013**, *9*, 263–272.
[54] a) V. Barone, M. Cossi, *J. Phys. Chem. A* **1998**, *102*, 1995–2001; b) M. Cossi, N. Rega, G. Scalmani, V. Barone, *J. Comput. Chem.* **2003**, *24*, 669–681.
[55] a) C. P. Kelly, C. J. Cramer, D. G. Truhlar, *J. Chem. Theory Comput.* **2005**, *1*, 1133–1152; b) M. Sparta, C. Riplinger, F. Neese, *J. Chem. Theory Comput.* **2014**, *10*, 1099–1108; c) F. Fantuzzi, M. A. C. Nascimento, B. Ginovska, R. M. Bullock, S. Raugei, *Dalton Trans.* **2021**, *50*, 840–849.
[56] Y. He, C. P. Souza, J. Weiser, M. Dietz, I. Krummenacher, R. D. Dewhurst, H. Braunschweig, F. Fantuzzi, J. Cui, *Eur. J. Inorg. Chem.* **2024**, e202400422.
[57] M. Elsner, *Physikalische Chemie I: Thermodynamik und Kinetik*, Springer, Heidelberg **2017**.
[58] J. Bresien, A. Schulz, M. Thomas, A. Villinger, *Eur. J. Inorg. Chem.* **2019**, *2019*, 1279–1287.
[59] a) T. M. Bockman, J. K. Kochi, *J. Am. Chem. Soc.* **1988**, *110*, 1294–1295; b) T. M. Bockman, J. K. Kochi, *J. Am. Chem. Soc.* **1989**, *111*, 4669–4683.
[60] a) M. Galvin, J. P. Guthrie, C. M. McDonnell, R. A. M. O'Ferrall, S. Pelet, *J. Am. Chem. Soc.* **2009**, *131*, 34–35; b) H. Schaeufele, D. Hu, H. Pritzkow, U. Zenneck, *Organometallics* **1989**, *8*, 396–401; c) T. A. Manuel, *Inorg. Chem.* **1964**, *3*, 1794–1796; d) W. Grimme, H. G. Koeser, *J. Am. Chem. Soc.* **1981**, *103*, 5919–5920; e) R. Aumann, H. Wörmann, *Chem. Ber.* **1979**, *112*, 1233–1251; f) T. T. Shi, Q.-S. Li, Y. Xie, R. B. King, H. F. Schaefer III, *New J. Chem.* **2010**, *34*, 208–214.

Version of record online: ■■, ■■

RESEARCH ARTICLE

A set of transition metal carbonyl complexes with a bismuth-ligand that bears an olefin functional group have been investigated. Visible-light-irradiation leads to CO elimination and concomitant coordination of the olefin moiety to the transition metal center in a chemically reversible process. Complexes featuring two bismuth-based ligands engage in oxidative addition/reductive elimination reactions of the corresponding dibismuthane, $R_2Bi–BiR_2$.

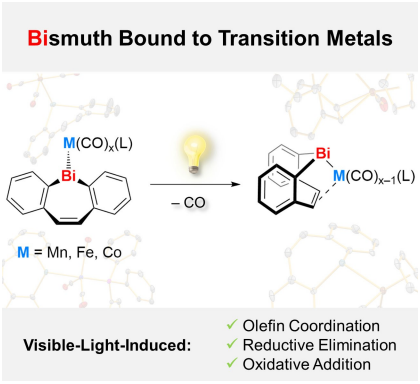

J. Ramler, F. Geist, C. Mihm, L. Lubczyk, S. Reith, C. Herok, F. Fantuzzi, C. Lichtenberg**